Learning-related contraction of grey matter in rodent sensorimotor cortex is associated with adaptive myelination

Tomás Mediavilla[a], Özgün Özalay[a], Héctor M. Estévez-Silva[a], Bárbara Frias[a], Greger Orädd[a], Fahad R. Sultan[a], Claudio Brozzoli[b], Benjamín Garzón[b,c], Martin Lövdén[b,c] and Daniel J. Marcellino[a]*

[a] Department of Integrative Medical Biology, Umeå University, 90 187 - Umeå, Sweden

[b] Aging Research Center, Department of Neurobiology, Care Sciences and Society, Karolinska Institute, 17 165 - Solna, Sweden

[c] Department of Psychology, University of Gothenburg, 405 30 - Gothenburg, Sweden

*Corresponding author

Materials & Correspondence:

Daniel J. Marcellino

Department of Integrative Medical Biology, Umeå University, 90 187 - Umeå, Sweden

Email: daniel.marcellino@umu.se

Abstract

From observations in rodents, it has been suggested that the cellular basis of learning-dependent changes, detected using structural magnetic resonance imaging (MRI), may be increased dendritic spine density, alterations in astrocyte volume, and adaptations within intracortical myelin. Myelin plasticity is crucial for neurological function and active myelination is required for learning and memory. However, the dynamics of myelin plasticity and how it relates to morphometric-based measurements of structural plasticity remains unknown. We used a motor skill learning paradigm to evaluate experience-dependent brain plasticity by voxel-based morphometry (VBM) in longitudinal MRI, combined with a cross-sectional immunohistochemical investigation. Whole brain VBM revealed non-linear decreases in grey matter (GM) juxtaposed to non-linear increases in white matter (WM) that were best modelled by an asymptotic time course. Using an atlas-based cortical mask, we found non-linear changes with learning in primary and secondary motor areas and in somatosensory cortex. Analysis of cross-sectional myelin immunoreactivity in forelimb somatosensory cortex confirmed an increase in myelin immunoreactivity followed by a return towards baseline levels. The absence of significant histological changes in cortical thickness further suggests that non-linear morphometric changes are likely due to changes in intracortical myelin for which morphometric WM volume (WMV) data significantly correlated with myelin immunoreactivity. Together, these observations indicate a non-linear increase of intracortical myelin during learning and support the hypothesis that myelin is a component of structural changes observed by VBM during learning.

Introduction

Longitudinal structural magnetic resonance imaging (sMRI) of the human brain has revealed experience-dependent local changes in estimates of grey matter volume (GMV)[1]. Recent evidence suggests that these grey matter (GM) changes follow a non-linear pattern[2]. The specific biological components that elicit these volumetric changes are not understood. From observations in rodents, it has been suggested that the cellular basis of changes detected using sMRI may, in part, be due to learning-dependent changes reported for increased dendritic spine density[3], alterations in astrocyte volume[4, 5], and adaptations within intracortical myelin[6-9]. Macroscopic plasticity of brain structure determined by sMRI has been directly associated with neuronal dendritic spine plasticity together with astrocyte reorganization in the absence of cell proliferation[3, 10], in which these plastic changes were observed to be transient. Furthermore, observations using two-session sMRI (before *vs*. after training), indicated macrostructural volumetric increases within areas involved in motor control, sensory processing, learning and memory[11]. At the microstructural

level, using *ex vivo* diffusion tensor imaging (DTI), significant white matter (WM) differences have been observed in WM underlying motor cortex[12] as well as experience-dependent DTI differences observed in GM structure[13]. Estimates of changes in GM using sMRI reflect a composite mixture of these biological changes. For example, changes in astrocytes or synaptic remodeling may explain changes in regional GMV. However, changes in intracortical myelin may also affect estimates of GMV, such that increases in intracortical myelin may reduce, and decreases in myelin may increase, estimates of GMV. Despite more recent developments of quantitative magnetic resonance imaging[14, 15], the mix and interplay between GM and WM changes that result in non-linear, experience-dependent, adaptive brain responses observed both in rodents and human studies remains unknown

Myelin plasticity is critical for learning and memory and myelin plasticity driven by both neuronal activity and experience has been described[16-21]. Active myelination by newly recruited oligodendrocytes, has been shown to be necessary for learning and memory[6, 22-24]. In addition, the learning of a novel skilled reaching task in rodents is associated with functional reorganization of cortical motor maps, including an expanded representation of the trained limb[25-27]. This functional remapping is accompanied by a variety of structural and functional changes, including synaptogenesis, increased spine formation, and glial changes[26, 28]. It was very recently described that learning in a forelimb skilled-reaching paradigm transiently suppresses oligodendrogenesis while increasing oligodendrocyte precursor cell (OPC) differentiation, oligodendrocyte maturation and myelin sheath remodeling in forelimb motor cortex[19]. Learning-induced suppression of oligodendrocytes was transient but left OPC differentiation unaffected, which suggests that learning may temporarily decrease survival and integration of differentiated OPCs as mature myelinating oligodendrocytes[19], in line with previous work in the developing CNS[29]. However, it is unknown whether adaptive myelination is restricted to discrete brain areas to enable fine-tuning of adaptive circuit responses. Furthermore, the temporal dynamics of myelin plasticity and how it relates to volumetric-based measurements of structural plasticity remains unknown.

In the present study, we used the single pellet skilled reaching task, a well-established paradigm for motor skill learning research in rodents[30], combined with longitudinal MRI and cross-sectional immunohistochemical analyses, to evaluate the time-course of experience-dependent brain changes and the related links between micro- and macrostructural changes. To analyze MRI data, we used voxel-based morphometry (VBM), a key technique to evaluate macroscopic changes in GMV that is frequently used to investigate a broad spectrum of neurological processes spanning from learning[11] and memory[3] to neurodegeneration[31, 32] and cognitive impairment[33]. This morphometric technique calculates voxel-wise estimates of GMV, and in the cortex, GMV is dependent upon local cortical thickness and surface area[34]. Studies in brain plasticity using sMRI

93 often rely on T1-weighted MR images that are sensitive to myelin, rendering the signal of a single
94 voxel highly dependent on the presence of myelin, thereby influencing the estimated volume.
95 Through longitudinal *in vivo* sMRI of rodent brain, using a specific MR sequence with a
96 magnetization transfer (MT) pulse to increase tissue contrast, we describe structural plasticity
97 dynamics during motor skill learning and the associated adaptive cortical myelination. This was
98 studied in *wild type* (WT) animals during learning of a skilled, single-pellet forelimb reaching task.
99 Plasticity in human brain structure have been typically assumed to follow a continuous linear or
100 asymptotic increase throughout the time of training. However, a recent study in humans revealed
101 GM expansion in motor cortex during the first 4 weeks of training followed by partial
102 renormalization[2]. In this study, we found that motor learning dynamically modulates
103 macrostructural brain plasticity, identified non-linear decreases in GMV juxtaposed to non-linear
104 increases in white matter volume (WMV) and that these changes are associated with adaptive
105 myelination in forelimb sensorimotor cortex.

106

107 **Results**

108

109 **Behavioral improvement after forelimb reach-and-grasp training**

110 A group of mice were trained (n = 39) each day on a forelimb-specific motor learning paradigm, the
111 single-pellet reaching task (SRT) over the course of 15 consecutive days (including 3 pre-training
112 days) and whole-brain structural images were acquired at six time points during the learning
113 paradigm (Fig. 1*A-C*; *SI Appendix*, Supplementary Video S1). Successful reaches and accuracy
114 during motor skill training significantly increased with time ($F_{11,364}$ = 25.50, P < .001 and $F_{11,364}$ =
115 7.976, P < .001, respectively) in trained mice (Fig. 1*D*, *E*). A higher level of skill was attained by the
116 group of trained mice compared to a group of non-trained controls (n = 16). The ability of control
117 mice to reach, grasp and retrieve pellets was measured on the final day of the motor learning
118 paradigm. At experimental day 14, trained animals successfully retrieved 47 ±3 % pellets with
119 accuracy of 18 ±3 % while non-trained control mice performed significantly lower (t = 8.641, df =
120 45, P < .001) than trained mice with only 7 ±2 % successful reaches and an average accuracy of
121 10 ±2 %.

122 An additional group of mice were trained (n = 64 + 8 from the previous group), yet individuals were
123 sacrificed at specific time points during the learning paradigm for cross-sectional analysis of brain
124 tissue. This group of trained mice showed similar improvements in successful reaches and
125 accuracy over the 12 days of training ($F_{11, 336}$ = 36.36, P < .001 and $F_{11, 336}$ = 5.806, P < .001
126 respectively; *SI Appendix,* Fig. S1*A*, *B*). On the final training day, trained animals that completed

the 15-day learning paradigm (n = 12) successfully reached-to-grasp an average of 54 ±5 % of pellets with an average accuracy of 22 ±3 %, whereas non-trained controls (n = 3 + 9 from the previous group) exhibited only an average of 7 ±2 % successful reaches with an average accuracy of 11 ±3 %. Skilled reaching performance of trained mice was significantly better than performance of non-trained control animals at the end of the behavioral paradigm (t = 7.425, df = 20, P < .001), confirming motor skill learning in trained mice.

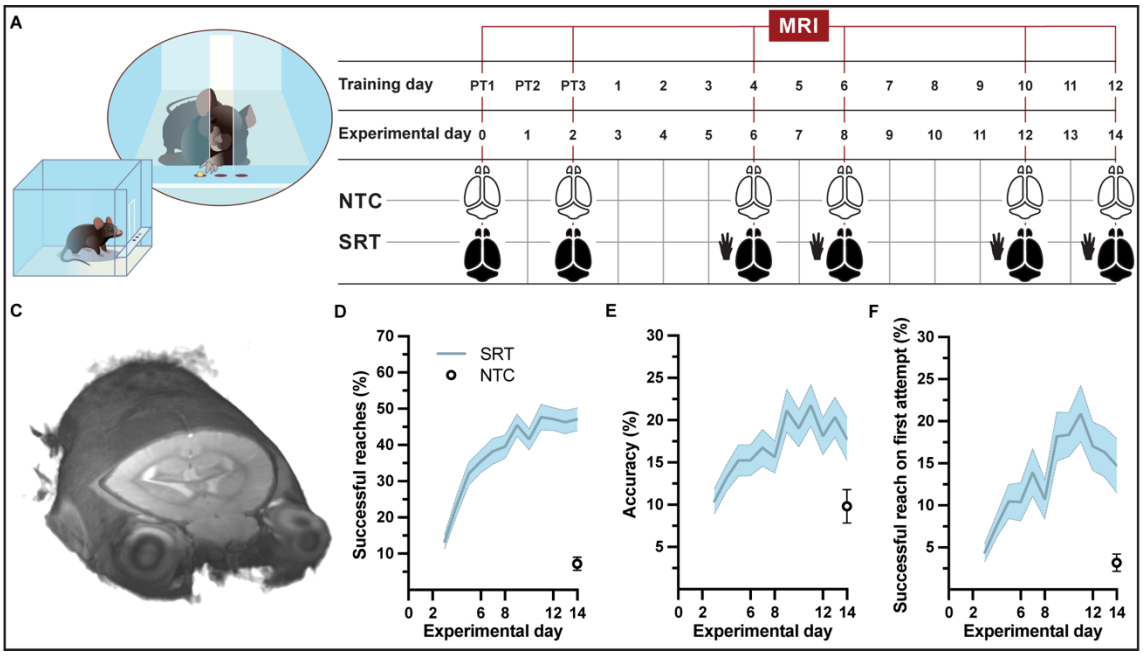

Figure 1. Experimental setup and forelimb reach-and-grasp skill learning. ***A***, ***B***, Illustration (***A***) and MR imaging timeline (***B***) during a motor skill behavioral paradigm (SRT: skill reaching trained; NTC: non-trained controls). ***C***, Example of an individual *in vivo* T1-weighted MRI at 9.4T at native resolution (0.1 mm isotropic, radiological display). ***D***, Mean performance scores during training of a skilled, single-pellet forelimb reach task, calculated as percentage (47± 1) of successful reaches (***D***) and percent (18 ± 1) accuracy (***E***) or percentage of successful reaches on the first attempted reach (19 ± 1) ***F***, during the 12-day training paradigm.

Whole-brain structural analysis identified non-linear decreases in grey matter volume juxtaposed to non-linear increases in white matter volume during motor learning

We performed *in vivo T1-weighted MR* imaging at baseline, immediately prior to motor skill training (last day of 'pre-training) and at four time points during motor skill learning ('training). VBM analyses revealed changes in GM and WM structure in trained and in non-trained control mice (*SI Appendix,* Fig. S2*A*, *B*; Supplementary Table S1). To discriminate the effects of motor learning from those of time, the learning effects were evaluated using whole-brain VBM analysis of longitudinal sMRI data on trained mice relative to non-trained controls (*i.e.*, group by time interactions). Three different

regression models (linear, asymptotic and quadratic), representing three different time courses, were used and revealed statistically significant changes in both GMV and WMV ($P_{FDR\ corr} < 0.01$). Significant non-linear decreases in GMV relative to the control group were observed juxtaposed with significant non-linear increases in WMV during learning (Fig. 2A, B). Interestingly, the asymptotic model provided a much higher number of significant voxels than either the linear or quadratic models and there were no significant linear changes in WM associated with learning (Table 1). Areas well-known to be involved in motor learning were identified by VBM analysis, following an asymptotic time course model in trained animals relative to non-trained controls (*SI Appendix*, Fig. S3). Significant decreases in GM and significant increases in WM were observed in both cortical and subcortical brain areas.

Table 1. Grey and white matter training by group interaction effects. Whole-brain between-group analysis presenting the significant number of voxels ($P_{FDR\ corr.} < 0.01$ and < 0.001) together with the change in volume (mm^3).

	grey matter (GM) changes			white matter (WM) changes	
	increase	decrease		increase	decrease
$P_{FDR\ corr} < 0.01$					
Linear	-	45158 (23.12)		12407 (6.35)	-
Asymptotic	-	241549 (123.68)		78442 (40.16)	-
Quadratic	-	28615 (14.65)		2250 (1.15)	-
$P_{FDR\ corr} < 0.001$					
Linear	-	1834 (0.94)		-	-
Asymptotic	-	109811 (56.22)		22095 (11.31)	-
Quadratic	-	2780 (1.42)		288 (0.15)	-

In addition, whole brain analysis indicated that, in some brain areas, one model fit the time courses better than the others. Akaike information criterion (AIC) values were used to distinguish these specific areas. Clusters for which AIC values indicated asymptotic modelling revealed GM decreases in discrete brain areas including primary motor cortex (MOp), primary somatosensory cortex for the forelimb (SSp-ul) and globus pallidus (GPe) (Fig. 2*C*). Whereas clusters for which AIC values indicated preferred quadratic modelling revealed GM decreases in the paramedian lobule (PRM) and vermian lobule VI of cerebellum (DEC), superior colliculus (SC) and nucleus accumbens (ACb; Fig. 2*D*).

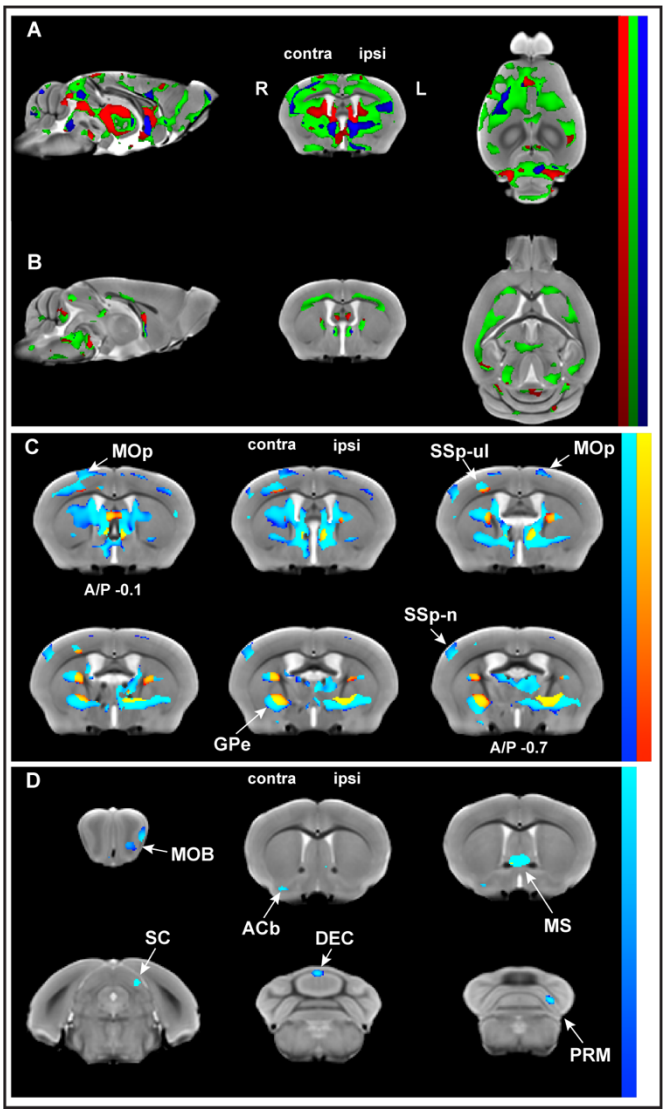

Figure 2. Whole brain structural analysis revealed non-linear decreases in grey matter volume juxtaposed to non-linear increases in white matter volume with learning. Changes in GM (***A***) and WM (***B***) volumes modelled by three different time courses (linear model in red, asymptotic model in green, and quadratic model in blue) overlayed on the *in vivo* MRI template created from this study. The decreases in GM volume (cold blue scale) and the increases in WM volume (warm red scale), in coronal sections ranging from A/P Bregma -0.1 to -0.7 mm, defined using the asymptotic model ($P_{FDR\ corr} < 0.01$) and thresholded at $\Delta_{AIC} > 10$ for asymptotic versus linear and/or quadratic models (***C***). Cortical and subcortical areas following an asymptotic model displaying GM decreases include primary motor cortex (MOp), primary somatosensory cortex for the forelimb (SSp-ul) and globus pallidus (GPe) contralateral to the trained limb, among others. Clusters for which AIC values indicated a preferred quadratic model (***D***). Preferred quadratic clusters are observed in the paramedian lobule of cerebellum (PRM), superior colliculus (SC) and main olfactory bulb (MOB) ipsilateral to the trained limb, medial septum and vermian lobule VI (DEC), and nucleus accumbens (ACb) contralateral to the trained limb.

VBM restricted to cortical sensorimotor areas identified non-linear decreases in grey matter volume together with non-linear increases in white matter volume during motor learning

To explicitly investigate changes within cortical regions known to be involved in motor-skill learning, based on previous observations, we generated a bilateral atlas-based mask of primary motor cortex (MOp), secondary motor cortex (MOs) and primary somatosensory cortex (SSp) (Fig. 3*A, B*). Using this cortical mask, the three different regression models were tested and compared (Table 2). This analysis demonstrated that asymptotic modelling was clearly preferred and that statistically significant decreases in GMV ($P_{FDR\ corr} < 0.001$) overlapped with significant increases in WMV ($P_{FDR\ corr} < 0.01$) in trained animals relative to non-trained controls (Fig. 3*A, B*). These were observed in primary motor areas (MOp) and somatosensory cortex for forelimb and hindlimb (SSp-ul and SSp-ll) contralateral to the trained limb, somatosensory barrel field (SSp-bf) ipsilateral to the trained limb, and bilateral secondary motor areas (MOs) and bilateral somatosensory area for the mouth (SSp-m). Additionally, we found GM decreases in contralateral somatosensory area for the nose (SSp-n) and bilateral GM decreases in primary motor areas (MOp) and somatosensory cortex for the forelimb and hindlimb (SSp-ul and SSp-ll), as well as in barrel field (SSp-bf). Furthermore, we observed bilateral increases in WMV in primary motor area (MOp), somatosensory cortex for the forelimb and hindlimb (SSp-ul and SSp-ll), somatosensory area for the barrel field (SSp-bf) and somatosensory area for the nose (SSp-n).

Table 2. Grey and white matter training by group interaction effects. Masked cortical areas (MOp + MOs + SSp) between-group analysis presenting the significant number of voxels ($P_{FDR\ corr.} < 0.01$) together with the change in volume (mm^3).

	grey matter (GM) changes			white matter (WM) changes	
	increase	decrease		increase	decrease
			$P_{FDR\ corr} < 0.01$		
Linear	-	-		-	-
Asymptotic	-	33817 (17.31)		13356 (6.83)	-
Quadratic	-	-		-	-

To further constrain our analysis, structural data were extracted and analyzed using a non-biased volume of interest (VOI) for sensorimotor cortex, based on fMRI maps of forepaw stimulation reported by Jung and colleagues in 2019[35] (Fig. 3*C, D*). Non-linear decreases in GMV and increases in WMV relative to non-trained controls were observed contralateral to the trained limb. These changes followed a non-linear model rather than a linear one (Δ AICc > 2; Table 3). In

addition, we created two additional VOIs based on known areas of reorganization of forelimb representation using multielectrode recordings and skill reaching[27]. Structural data were extracted and plotted for the caudal forelimb area (CFA) and the rostral forelimb area (RFA) contralateral to the trained limb (Table 3; *SI Appendix,* Fig. S4) and similar non-linear changes were observed. Changes in both GMV and WMV followed a quadratic/non-linear pattern rather than linear (Δ AICc > 2) except for WM in RFA where it was not possible to discriminate which model fit best (Δ AICc < 2).

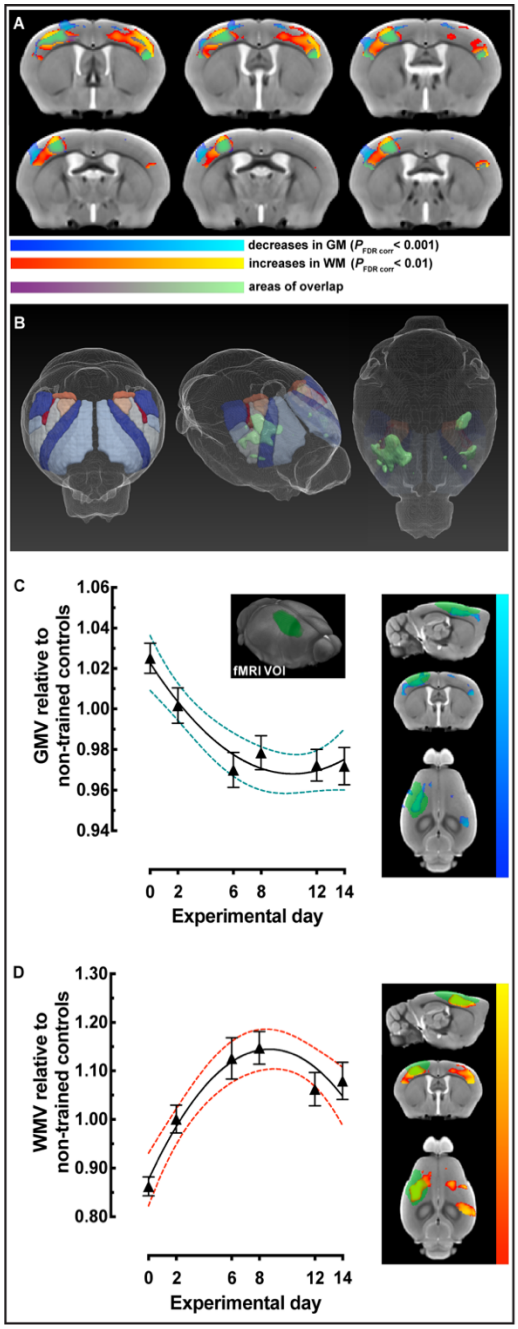

Figure 3. Sensorimotor-restricted VBM analysis in cortex identified non-linear decreases in GMV together with non-linear increases in WMV during motor learning. *A*, VBM analysis using an atlas-based bilateral mask for primary motor cortex (MOp), secondary motor cortex (MOs) and primary sensory areas (SSp) revealed significant decreases in GMV (cold blue scale) and increases in WMM (warm red scale) following an asymptotic model ($P_{FDR\ corr} < 0.001$ and < 0.01, respectively). ***B***, 3D representations of the atlas-based mask for MOp+MOs+SSp together with the overlap of significant GMV and WMV changes (green). ***C*,** GMV changes, relative to non-trained controls, in sensorimotor cortex contralateral to the trained forelimb extracted using a VOI based on fMRI mapping of forepaw stimulation (VOI represented in green). ***D*,** WMV changes, relative to non-trained controls, from the same VOI in ***C***. Non-linear decreases in GMV are observed together, and overlap, with non-linear increases in WMV.

Motor learning evokes non-linear plasticity of cortical white matter components that are associated with adaptive myelination

Although we employed a T1-weighted sequence specifically chosen for increased myelin detection within GM, MRI metrics do not provide direct myelin measures. We therefore immunolabelled myelin basic protein (MBP) in coronal brain sections at six different intervals during the learning paradigm (*SI Appendix,* Fig. S5*A*). These intervals were matched to those used for MRI: baseline, immediately prior to motor skill training and at four time points during motor skill training. Myelin immunoreactivity was quantified in an area of SSp-ul that presented with a highly significant VBM cluster contralateral to the trained limb, as well as significant changes in ipsilateral SSp-ul when an atlas-based cortical mask was applied to our data (Fig. 4*A*). We observed a significant correlation between WMV, extracted using an unbiased fMRI-based VOI from an independent study[35], with myelin immunoreactivity in trained animals (Fig. 4*B*; Pearson's $r = .75$, $P = .03$). In line with this result, we found a non-significant trend between GMV and myelin immunoreactivity (Fig. 4*B*; Pearson's $r = -.38$, $P = .35$). The quantification of myelin immunoreactivity within the bilateral cluster located in SSp-ul revealed significant changes with training (one-way ANOVA, $F_{5,62} = 2.333$, $P < .05$; Fig. 4*C*). Specifically, myelin immunoreactivity increased up until experimental day 6 after which it began to decrease towards baseline levels. From baseline measurements, at experimental day 0, average MBP immunoreactivity increased by 15 % at experimental day 6 followed by an 8 % decrease from experimental day 6 to experimental day 14. In line with our observations using VBM, the differences detected in myelin immunoreactivity preferentially followed a non-linear model rather than linear (Δ AICc > 2) with an 87.8 % probability of a preferred non-linear model compared to a linear model. No significant differences were observed in myelin immunoreactivity between trained animals and non-trained controls at experimental day 14 ($t = 0.4096$, df = 22, $P > .05$) (*SI Appendix,* Fig. S6*A*) nor in non-trained controls between baseline experimental day 0 and experimental day 14 (*SI Appendix,* Fig. S6*B*).

In addition to myelin immunoreactivity, cortical thickness was also quantified in histological sections in sensorimotor cortex where myelin was evaluated (Fig. 4*D-F*). No significant difference was observed in cortical thickness between trained mice and non-trained controls ($t = 0.5561$, df = 98, $P > .05$, n animals = 72 for trained mice, n animals = 28 for non-trained controls). Similarly, no

difference was found in the cumulative distribution of cortical thickness between groups (*K-S test,* $P > .05$, $D = 0.08949$, $n = 424$ for trained mice, $n = 191$ for non-trained controls).

Table 3. Comparison of AIC values for changes in grey and white matter taken from structural data extracted using three unbiased cortical volumes.

Grey matter (GM) changes						
	fMRI VOI		RFA VOI		CFA VOI	
	Linear	Quadratic	Linear	Quadratic	Linear	Quadratic
AICc	-1271	-1278	-1833	-1835	-1337	-1358
probability of correctness	3.50%	96.50%	24.09%	75.91%	<0.01%	>99.99%
White matter (WM) changes						
	fMRI VOI		RFA VOI		CFA VOI	
	Linear	Quadratic	Linear	Quadratic	Linear	Quadratic
AICc	-664.3	-686.6	-94.80	-95.33	-682.2	-699.8
probability of correctness	<0.01%	>99.99%	43.45%	56.55%	0.02%	99.98%

Morphometric changes in WMV and myelin immunoreactivity in SSp-ul were observed to follow a non-linear trajectory in which we observed significant increases followed by a total, or partial, return to baseline levels during skill learning. To explore the relationship between learning and adaptive myelination, we evaluated whether learning rate correlates with the asymptotic changes for the WMV. We evaluated WM data extracted from the fMRI VOI contralateral to the trained limb at experimental day 14 and found a correlation between learning rate and WMV (Fig. 4*G*) (Pearson's $r = - 0.378$, $P = 0.0360$). Animals in which changes in WMV presented a larger similarity to an asymptotic time course (lower AICc values) exhibited a higher learning rate.

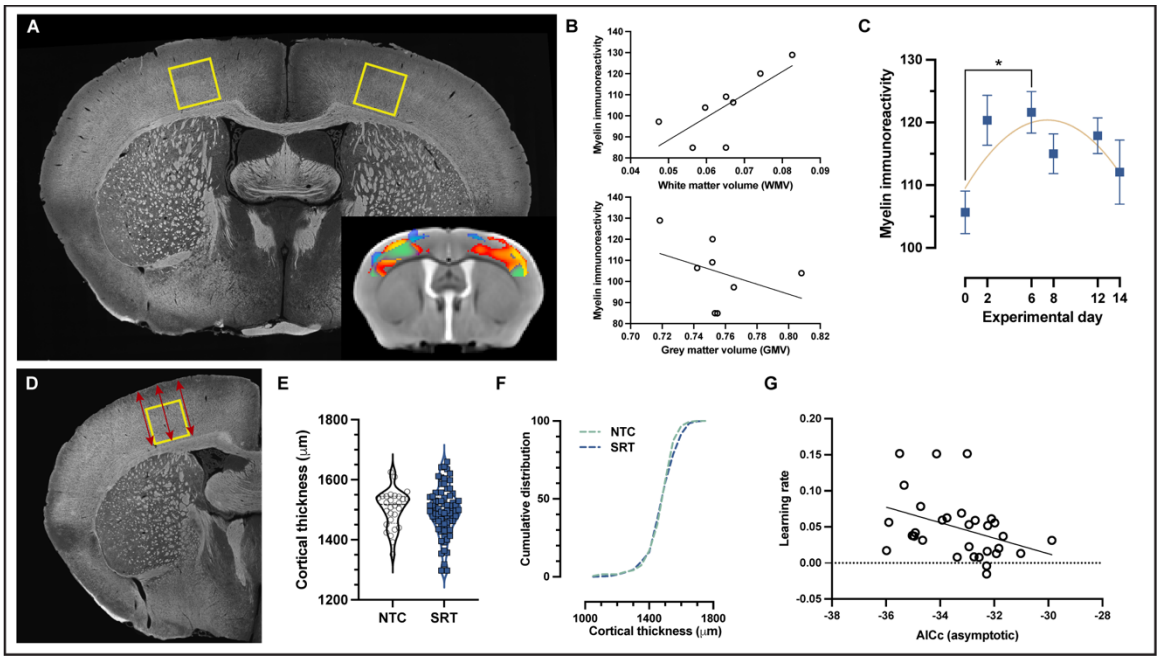

Figure 4. Motor learning evokes non-linear plasticity of cortical white matter components that are associated with structural changes. ***A***, Representative image of myelin immunohistochemistry. ***B*****,** Positive correlation between cortical WMV values and myelin immunoreactivity at the individual level in trained animals (Pearson's r = .75, *P* = .03) and non-significant negative correlation between GMV and myelin immunoreactivity (Pearson's *r* = -.38, *P* = -.35). ***C*****,** Myelin immunoreactivity increases until experimental day 6, after which it decreases towards baseline levels. The changes detected in myelin immunoreactivity follow a quadratic model rather than a linear one (AICc > 2). Data are represented as mean ± s.e.m. ***D*****,** Illustrative representative of the three measurements acquired at the sensorimotor cortex in the same area where myelin was quantified. ***E***, No significant changes were observed in sensorimotor cortical thickness between trained animals and non-trained controls and no differences in the cumulative distribution of cortical thickness were observed between groups in SSp-ul (***F***). ***G*****,** Correlation between learning rate and the asymptotic fit (measured as AICc) for WMV on an individual level (Pearson's r = - 0.378, *P* = 0.0360) in which animals with WMV that best fit an asymptotic model (lower AICc values) exhibited higher learning rates.

Discussion

Myelination, like synaptic plasticity, contributes to learning by activity-dependent modification of an initially 'hard-wired' circuitry[36]. The dynamics of myelin plasticity and how it relates to volumetric-based measurements of experience-dependent brain changes remain unknown. In this study, we combined motor skill learning in mice with longitudinal sMRI and immunohistochemistry to study the nature of structural changes that take place in the brain during learning.

Longitudinal *in vivo* sMRI acquired throughout learning a skilled, single-pellet forelimb reach task revealed bilateral non-linear decreases in GM juxtaposed to non-linear increases in WM modelled

by an asymptotic time course function. Specifically, using an atlas-based cortical mask, we found bilateral non-linear changes with learning in primary and secondary motor areas and in somatosensory cortex. Supporting these results, a cross-sectional analysis unveiled an increase in myelin immunoreactivity in the somatosensory cortex for the forelimb, followed by a return towards baseline. The complementary cortical thickness analysis did not reveal any significant difference between trained animals and non-trained controls. This multimodal approach indicates that non-linear changes observed in cortical GM and WM using VBM are likely caused by changes in tissue composition (*e.g.*, more intracortical myelin, as suggested by the immunodetection analyses) rather than changes in cortical thickness or surface areas of SSp-ul, which are unlikely to happen in the relatively short period of a 15-day learning paradigm. These results are further corroborated by the additional finding of a significant correlation between morphometric WMV and myelin immunoreactivity in the same cortical area. Therefore, WMV calculated from segmented T1-weighted MRI using an MT pulse represents myelin to a substantial degree. Altogether, these observations indicate a non-linear increase of intracortical myelin with learning.

Consistent with this idea, oligodendrocyte development has been reported to be required for motor learning in adult mice within the first hours after being introduced to the complex wheel running learning paradigm[37]. Furthermore, a recent study demonstrated that forelimb-skill reaching dynamically modulates myelination through oligodendrocyte precursor cell (OPC) differentiation[19]. As well, the non-linear changes observed in somatosensory cortex for the forelimb match with the well-characterized reorganization of forelimb representation during motor skill learning using electrophysiological measurements[27].

As previously described in humans[2], and in mice[11], our *in vivo* morphometric analysis revealed bilateral changes in several brain regions, including SSp-ul. While structural changes contralateral to the trained forelimb were expected, strong cortical changes ipsilateral to the trained limb are still controversial. Changes in ipsilateral motor cortices are consistent with fMRI findings in humans showing bilateral MOp activation during the execution of a unilateral high-precision motor task[38]. This bilateral activation was later attributed to an inhibitory effect from ipsilateral motor cortex on contralateral motor cortex. Interestingly, this inhibitory effect was modulated by the demand on accuracy of the motor task[39]. Thus, ipsilateral changes in GM and WM with learning, may be attributed to existing interhemispheric connectivity that is enhanced and re-wired during learning, or possible enhanced ipsilateral inhibitory activity may also lead to changes in volume.

In contrast with our findings of GMV decreases, the study of experience-dependent volumetric changes in primary motor cortex in human adults, trained to write and trace with their non-dominant hand, revealed a bilateral GMV expansion followed by a partial renormalization[2]. It is possible that the different motor skill learning paradigm used here triggered different structural changes in the brain. On the other hand, these differences could also be attributed to the use of a higher

magnetic field in mice than in humans (9.4T *vs*. 3T, respectively) or, perhaps most likely, a consequence of the MRI sequence, optimized for an enhanced detection of myelin. The use of *in vivo* sMRI in mice using two-session sMRI (before *vs*. after training) unveiled significant enlargements in GMV in multiple brain regions[11]. In addition, rodent studies using *ex vivo* DTI with similar motor skill paradigms, reported an overall increase in WM in cerebellum[11] and in corpus callosum directly below primary motor cortex[12] after either 23-27 and 11 days of training, respectively. These studies were limited to trained animals versus non-trained control animals at endpoint and therefore, it is not possible to draw conclusions regarding the temporal dynamics of brain plasticity with learning.

The WM enlargement we observed by VBM and by myelin immunohistochemistry exhibits an initial expansion, followed by a (partial) renormalization. These observations support the hypothesis that myelin is, at least in part, a component of an expansion-renormalization model comprising exploration, selection, and refinement stages[40-42]. It is likely that newly formed connections are strengthened in response to repetitive firing of neural circuits produced by a discrete sequence of movements[43]. The increased activity within these circuits likely stimulates additional myelination of involved axons to provide increased efficiency. Experiments utilizing two-photon imaging after inducing monocular deprivation revealed neuron-class specific myelin plasticity, suggesting that reconfiguration of network connectivity after sensory deprivation requires precise tuning of individual myelination profiles instead of a broad addition of myelin[44]. Thus, the exploration phase of learning involves an expected rise in myelination during initial motor skill improvement, or acquisition. In later stages of motor learning, optimal circuitry is selected to perform the motor task that is subsequently refined through reinforcement and the non-efficient candidate circuits are pruned away[45]. Interestingly, once the optimal circuitry is selected and refined, active myelination is no longer required to support recall and execution of a pre-learned skill[6]. Our whole brain analysis comparing the different possible time-course models identified that the majority of structural changes with learning follow a non-linear pattern, suggesting that expansion followed by (partial) renormalization is a rather general phenomenon across regions and may be a common principle that unites many manifestations of structural plasticity. Moreover, there is an interestingly large, yet non-significant increase in myelin immunoreactivity during the pre-training days, suggesting that pre-training and task familiarization is sufficient to trigger formation of new neuronal connections, stimulating myelination. Consistent with this idea, a previous study in mice showed that the proliferation of OPCs was accelerated in motor cortex within just 4 hours of exposure to the complex wheel. In addition, the introduction to a novel skill learning paradigm stimulated OPC differentiation into newly-forming oligodendrocytes after just 2.5 hours of self-training[37]. Although previous results using the single-pellet reaching task[19] suggested that production of myelin does not appear until days or weeks later (for Review see[46]), here we observe that myelination is a rapid and dynamic plastic change throughout learning.

Higher learning rates were associated with a non-linear/asymptotic model of the changes in the MRI-derived WMV. We could speculate that the selection and refinement phases of the expansion-renormalization model highly influence the proficiency of learning at the individual level. During the exploration phase, a large production of candidate circuits that could potentially elicit effective movements takes place, increasing myelination/myelin levels. However, the magnitude of increase in candidate circuits does not imply a better performance. With a large pool of candidate circuits, the serial activation of the different candidate circuits could lead to behavioral variability (a wide range of diverse performances). Nevertheless, the selection and reinforcement of the circuits that can reliably produce the target movement and the pruning of the non-efficient candidates to carry out the task leads to a decrease in myelin levels and appears to be related with higher learning rates. Decreasing the number of circuits reduce the behavioral variability and ~~could~~ imply a better performance.

VBM, a method that has been widely used during the past two decades to identify and characterize brain changes among populations, is used to detect systematic density differences of a particular tissue class. In VBM, each voxel in smoothed images contains the average amount of GM around that voxel[34]. Although modulated GM density (mGM) and cortical thickness are completely different measures, both are commonly used to assess GMV. However, Chung and colleagues found discordances between mGM and cortical thickness analyses[47]. A strong correlation between T1-weighted signal intensity and mGM was reported while no correlation was found between signal intensity and cortical thickness. In cortical VBM, if each voxel is a combination of mGM density, cortical thickness and surface area, the interpretation of VBM results as volume alone is not entirely correct. Since we did not find significant changes in cortical thickness during learning and that it is unlikely that changes in surface area were produced during the 15-day learning paradigm, we can assume that the morphometric changes observed during learning are consequence of changes in GM and WM density and not volume. Furthermore, this assumption is in line with the changes we observed in myelin immunoreactivity at the histological level.

In this study, we observed the temporal dynamics of experience-dependent macrostructural brain changes during motor skill learning, identified non-linear decreases in grey matter volume juxtaposed to non-linear increases in white matter volume, and found that these changes are associated with adaptive myelination in forelimb sensorimotor cortex. Our results empirically back up the idea that myelination is a rapid initial and partly transient plastic change in learning and support the use of VBM on WM structural data to evaluate myelinated fibers in cortex.

Materials and Methods

Experimental design. To study the structural changes that occur in the brain during the acquisition of a novel motor skill, two independent sets of experiments were performed:

i) Motor skilled training was combined with *in vivo* longitudinal sMRI: trained animals (SRT, *n* = 39) and non-trained control animals (NTC, *n* = 16) were scanned at PT1 (baseline), PT3, T4, T6, T10 and T12 (Fig. 1*B*). Animals were sacrificed at endpoint (T12).

ii) Motor skilled training was performed and animals at different time points during the learning paradigm were sacrificed for a cross-sectional evaluation of myelin immunoreactivity (Fig. 4A). For the SRT group, 12 animals were sacrificed at PT1, PT3, T4, T6 and T10 and 4 animals at T12. For the NTC group, 3 animals were sacrificed at T12. Tissue from animals sacrificed at endpoint (T12) from *i)* above were also used for evaluation of myelin immunoreactivity (8 trained animals and 9 non-trained controls for a total of 12 animals per time point).

Animal care. All procedures were in accordance with protocols approved by the Umeå Regional Ethics Committee for Animal Research (ethical permit: Dnr A 35/2016). A total of 123 young-adult (8- to 11-week-old) male C57BL/6J mice (Jackson Laboratory, Bar Harbor, ME, USA) were used in the study. Animals were housed in a 12-h/12h light-dark cycle under controlled humidity and temperature (23°C). During initial acclimation after delivery, animals were provided food and water *ad libitum*. All animal handling and behavioral training was carried out during the light phase of the light-dark cycle**.** Mice were food restricted one week prior to behavioral training. Food restriction was performed gradually to reach 85-90 % of their free-feeding weight (calculated by a non-food-restricted control group). To familiarize mice with the precision pellets (20 mg Purified Rodent Tablet, TestDiet, Richmond, IN, USA) used during motor skill training, 1 g pellets/day were placed into the homecage on the two days prior to pre-training. Animal weight was monitored during the entire experiment to ensure that individuals did not fall under 85 % of their calculated free-feeding weight on an individual basis.

Behavioral training - Single-pellet Reaching Task. A skilled, single-pellet forelimb reach paradigm was performed as previously described in rat[48] with some modifications to the training cage (26.5 cm x 9 cm x 20 cm; with grooves to position pellets located 1 cm from inside the cage, see Fig.1*A*). Mice were trained to reach through a narrow slit to grasp and retrieve food pellets positioned within a small indentation located contralateral to the preferred forelimb for each individual animal. Prior to motor skill training, mice were handled and habituated to the behavioral cage during three days ('pre-training'; 3 days of 15-min sessions). During the first pre-training day, pellets were placed onto the floor close to the narrow opening at the front of the training cage. During the second and the third pre-training days, pellets were placed onto the shelf located at the front of the cage, outside of the narrow opening and animals occasionally reached to grasp pellets which was used to determine handedness. During the subsequent 12 days ('training'; 12

453 consecutive days of 15-min sessions), each animal in the trained group was given a 15-minute
454 training session each day that consisted of 30 discrete trials (one pellet/trial). During the entire 15-
455 day experimental paradigm, age-matched non-trained control mice (*n* = 16) were placed into
456 identical training cages for 15 minutes and were provided 30 pellets on the cage floor for each
457 experimental day.

458 **Behavioral analysis.** Each of the 12 training sessions were recorded using a digital camera
459 positioned at the front of the training cage. To evaluate motor performance, the number of
460 successful reaches were tallied in addition to the total number of grasping attempts per trial. Video
461 recordings were reviewed if clarification of the score was required. Grasp-to-reach success was
462 calculated as the percent of trials for which food pellets were successfully retrieved from the groove
463 without exhibiting any abnormal behavior (*i.e.*, reaching with the non-trained forelimb, or the use of
464 tongue to retrieve to pellet) divided and normalized by the number of trials completed by each
465 individual animal during the 15-minute daily training session. Accuracy was calculated as the
466 percentage of successful reaches normalized by the number of attempts performed for each
467 successful trial. The learning rate for each individual was calculated by the slope of a logarithmic
468 model fitted to the learning curve for each individual animal. To evaluate a possible improvement
469 in successful reaches and accuracy over time, restricted maximum likelihood (REML) analysis
470 (allowing for missing values from the animals sacrificed at different timepoints during the learning
471 paradigm) was calculated for the SRT group. To compare the performance of the SRT group and
472 NTC group we carried out a t-test analysis on successful reaches at experimental day 14.

473 **MRI.** Animals were scanned and at least 2 h transpired after waking from anesthesia to behavioral
474 training on any of the MR scan days along the experimental timeline. To prevent any possible
475 isoflurane-induced memory impairment, mice were administered a very low dose (0.7 mg/kg, *s.c.*)
476 of the highly selective α_5GABA$_A$ receptor inverse agonist, L-655,708 (Sigma-Aldrich, Stockholm,
477 Sweden AB) 15 min prior to the induction of anesthesia[49]. Anesthesia was induced using 4.0 %
478 isoflurane mixed with oxygen that was subsequently lowered to 1.5 - 2 % for maintenance during
479 experimental scans. T1-weighted images were acquired using a magnetization transfer (MT) pulse
480 for increased contrast between tissue types with different transfer susceptibilities. We used a T1
481 3D FLASH sequence (TR/TE = 50/8 ms, flip angle = 20°, using 4 repetitions) with MT-weighting by
482 Gaussian-shaped off-resonance irradiation (30 μT MT pulse, frequency offset 1.5 kHz, pulse
483 duration 1.8 ms, flip angle 351.2°) performed at 9.4 T (Bruker BioSpec 94/20, running Paravision
484 6.0 software) with 100 μm isotropic spatial resolution using a 1H Quadrature transmit/receive MRI
485 cryogenic mouse brain RF coil (MRI CryoProbe, Bruker, Germany) for signal reception. The total
486 scan time was 38 min. At the end of each scan, mice were administered saline (10 mL/kg, *i.p.*) for
487 rehydration and individually placed into a cage to recover from anesthesia before it was returned
488 to its homecage.

MRI Data Preprocessing Analysis. T1-weighted images were reoriented to match FSL standard orientation convention and were skull stripped using a template-based approach[50]. Skull stripped images were then bias-corrected for intensity inhomogeneities using the N4 Bias Correction algorithm included in ANTs software package[51].

Bias corrected, skull stripped brains were manually realigned in SPM8 to approximate the orientation of the stereotaxic, population-averaged, tissue-segmented *in vivo* brain templates for *wild type* C57Bl/6 mice; described and provided in Hikishima *et al.*, 2017[52]. The origin was also set to match the template. The longitudinally acquired scans for each subject were registered using serial longitudinal registration SPM12 to create an average image for each subject. These averages were then used to create a brain template encompassing all subjects using a serial longitudinal registration of the average from each subject (*SI Appendix*, Fig. 7*A, B)*. Our study-specific template was subsequently coregistered and resampled (from 0.1 to 0.08 mm isotropic resolution) to C57Bl/6 template provided in Hikishima *et al.*, 2017[52]. Next, the individual scans, from all subjects and timepoints, were coregistered and resampled to the *in vivo* study-specific brain template at 0.08 mm isotropic resolution.

A two-stage process was used create our own study- and sequence-specific tissue probability maps (TPMs) based on the grey matter (GM), white matter (WM), and cerebrospinal fluid (CSF) TPMs provided together with the *in vivo* C57Bl/6 template provided in Hikishima *et al.*, 2017. The pre-process segmentation tool from the SPMmouse toolbox[53] (SPM8) was used for the serial longitudinal average of 44 subjects, for which both handedness and training were balanced among the 44 subjects, to create preliminary TPMs from our data. The data were segmented into GM, WM, and CSF images using a mixture of Gaussians and tissue probability maps (TPMs) in SPMmouse. An initial study-specific *in vivo* brain template was created using the DARTEL toolbox of SPMmouse, which improves registration with an inverse consistent, diffeomorphic transformation. This process was repeated a second time, segmentation followed by DARTEL, but using the preliminary TPMs generated from the first DARTEL step to create our study- and MR sequence-specific tissue probability maps (TPMs; *SI Appendix*, Fig. 7*C*). These final TPMs were then used to segment the individual scans, from all subjects and timepoints. Modulated and normalized images of GM, WM and CSF were obtained with DARTEL, multiplied by the Jacobian determinants derived from the spatial normalization. The images were spatially smoothed by convolving with an isotropic Gaussian kernel (full width at half maximum) of five times the voxel size to minimize risk of false positives in statistical analysis.

The individual smoothed and modulated GM and WM tissue probability maps were thresholded at 0.2 (20%) to create GM and WM masks for removal of low probability voxels. All timepoint data for each subject were then concatenated into a single 4D image for further statistical analysis.

VBM Statistical Analysis. Linear Mixed Effects (LME) statistical approach was used to test our hypothesis on whether there are significant changes in GM and WM probabilities because of skilled training over time between trained and control groups. LME was chosen as it is capable of handling missing data and enables modeling of random effects in a longitudinal dataset. For this purpose, Total Intracranial Volume (TIV) and amount of training sessions (or time) were defined as fixed effects and subjects defined as random effects for intercept and time to analyze the data. We used R version 4.0.3 (R Core Team, 2017) with lme4 version 1.1-23[54] to perform LME analysis using an in-house coded R script on Ubuntu 18.04.05 LTS workstation. FDR correction was used to correct for multiple comparisons at $P<.05$ significance level.

To test for different patterns of change in GM and WM, we used three different regression models (and their opposite function) representing three different time courses; 1) Linear, 2) Increase followed by a stabilization (inverse-quadratic-asymptotic), and 3) Increase followed by a renormalization (inverse-quadratic) as depicted in *SI Appendix,* Fig. S8. We tested all three regression models for each subject in separate LME analysis to detect changes in GM and WM volumes, both between and within groups.

To study changes in GM and WM with learning specific to cortical areas, we restricted our analysis to M1, M2 and S1 regions using a mask based on the Turone Mouse Brain Template Atlas (TMBTA)[55] registered to our *in vivo* brain template.

Tissue processing and histology. Animals were anesthetized using 100 mg/kg pentobarbital sodium (*i.p.*, 60 mg/ml, Apotek Produktion & Laboratorier - APL, Kungens Kurva, SE) and transcardially perfused using Tyrode's solution followed by 4 % (w/v) paraformaldehyde (PFA) freshly prepared on the same day. After perfusion, brains were post-fixated in 4 % PFA at 4° C for 48 h. Then, PFA was removed and the brains were stored in phosphate buffer (PB) pH 7.40 containing 0.01 % (w/v) sodium azide at 4° C. Previous to histology, the brains were cryoprotected in 10 % (w/v) sucrose in PB (Na_2HPO_4 x $2H_2O$, Na_2HPO_4 x H_2O) with 0.01 % (w/v) sodium azide at 4° C. Brains were mounted in O.C.T compound (VWR chemicals, VWR International, Inc. US), snap frozen using high pressure CO_2 and sectioned coronally from Bregma AP 1.70 mm to AP -1.34 mm at 20 µm using a rotatory microtome cryostat (Microm Microtome Cryostat HM 500M). For each brain, at least 10 series of 3 slides (Superfrost Plus, Thermo Fisher Scientific, Waltham, MA, USA) each containing 6 sections per slide were obtained.

Immunofluorescent staining. Immunodetection of myelin was performed using anti-myelin basic protein on coronal sections ranging from Bregma AP -0.1 mm to AP -0.7 mm. Tissue sections were re-hydrated in PBS 0.1 M (Na_2HPO_4 x $2H_2O$, Na_2HPO_4 x H_2O + NaCl + KCl) and subsequently blocked using 5 % (v/v) goat serum in PBS containing 0.3 % Triton X-100 (PBST) for 1 hour at room temperature. Sections were then incubated with rat monoclonal anti-Myelin Basic Protein

primary antibody (1:400; Abcam - ab7349) in PBST containing 2 % (v/v) goat serum for 48 hours at 4° C in a humidified chamber. Sections were washed to remove primary antibody (PBS 0.1 M) and then incubated with fluorescently labelled secondary antibody (goat anti-rat Alexa Fluor 594; Invitrogen - Molecular Probes A21211) in PBST containing 2 % (v/v) goat serum for 1 h at room temperature in a humidified chamber. Secondary antibody was removed by washing with PBS 0.1 M and coverslips were mounted using Mowiol 4-88 (Sigma Aldrich, St. Louis, MO, USA) with 2.5 g/100 ml DABCO (Sigma Aldrich, St. Louis, MO, USA). Immunolabelled sections were stored at 4° C.

Image acquisition and quantification. Sections ranging from Bregma AP -0.1 mm to AP -0.7 mm for each animal (*n* = 84 animals; *n* = 211 sections), were selected for fluorescence-based microscopy imaging. Images were acquired using a TxRed filter (excitation = 540-580 nm; emission = 600-660 nm) on a Nikon Eclipse Ti-E inverted microscope with an DU897 ANDOR EMCCD camera controlled by Nikon NIS Elements interface, equipped with Nikon CFI Plan Apochromat 20x (N.A 0.75) objective. Prior to analysis, all the images were aligned using Amira-Avizo Software (version 6.3.0, Thermo Fisher Scientific, Waltham, MA, USA). A region of interest (ROI) was selected based upon a significant VBM cluster in SSp-ul described in this study. The ROIs were manually positioned and saved for each section using FIJI[56]. Signal to noise (specific myelin immunoreactivity versus background fluorescence) was determined by the segmentation of each image using FIJI's Multi Otsu Threshold plugin using three different levels of classification. This plugin is based on Otsu's original Method but also implements an algorithm described by Liao and Chung[57]. The specific signal was quantified for each section per individual to calculate a mean immunoreactive value for each subject (*n* = 12 per time point).

Cortical thickness analysis. Cortical thickness (layers I to VI) was measured in SSp-ul at the location of the ROI used to quantify myelin immunoreactivity. Three measurements were made in both hemispheres for each animal corresponding to the area of the significant cluster observed from whole-brain VBM analysis. The measurements were acquired from the length of three lines that were drawn based on the ROIs for myelin immunoreactivity. Data from 60 trained animals and 24 non-trained controls. In total, 424 measurements from trained animals and 191 measurements from non-trained animals were used. Data from any images in which cortex was partially damaged, confounding a proper measurement, were not included.

Statistical analysis. Student's T-test was used to compare two groups and One-Way ANOVA with Tukey's test for multiple comparisons. Akaike's Information Criterion was used to calculate the goodness of fit. The probability of correctness for a model was computed using the next equation: probability = $e^{0.5\Delta}/1+e^{0.5\Delta}$ where Δ is the difference between the AICc values. Figure legends specify the statistical test used in each case and the number of independent measurements (*n*) evaluated.

595 Behavioral improvement, myelin immunoreactivity mean intensities and cortical thickness were
596 analyzed using Prism 9.0.0 for macOS (GraphPad Software, San Diego, California USA).

597

598 **Acknowledgments**

599

600 This work was supported by Umeå University Medical Faculty, Umeå Sweden (D.M.); StratNeuro,
601 Umeå University, Umeå Sweden (D.M.); Swedish Research Council, Stockholm, Sweden (Grant
602 2018-01047) (M.L.); Kempe Foundation, Örnsköldsvik, Sweden (Grant JCK-1922.2) (D.M., F.S.);
603 *Insamlingsstiftelsen för medicinsk forskning* 2019 (D.M.); *Magnus Bergvalls Stiftelse*, Stockholm,
604 Sweden (Grant 2016-01639) (D.M.); Swedish Research Council, Stockholm, Sweden (2015-
605 01717) (C.B.); Agence Nationale pour la Recherche (ANR-16-CE28-0008-01) (C.B.). H.M.E-S was
606 supported by a grant from the *Agencia Canaria de Investigación, Innovación y Sociedad de la*
607 *Información* (ACIISI) of the *Regional Consejería de Economía, Industria y Comercio*, Canary
608 Islands Government and European Social Fund [Canarias 2014-2020, Axis 3 Priority Theme 74
609 (85%)]. We also would like to acknowledge the Small Animal Research and Imaging Facility
610 (SARIF) at Umeå University for providing the MRI equipment to perform the study and the
611 Biochemical Imaging Center at Umeå University (BICU) and National Microscopy Infrastructure,
612 NMI (VR-RFI 2019-00217) for providing assistance in microscopy. With great appreciation, we also
613 thank Dr. Seong-Gi Kim and Dr. Won Beom Jung for providing the mask of the fMRI-based
614 sensorimotor cluster reported in Jung *et al*., NeuroImage, 2019.

615

616 **Competing Interest Statement:** The authors declare no competing interests.

617

618 **Author Contributions:** T.M., H.M.E-S., C.B., M.L. and D.J.M. designed research; T.M., H.M.E-S,
619 B.F., and D.J.M. performed research; T.M., Ö.Ö., G.O., F.R.S., B.G., and D.J.M. analyzed data;
620 T.M. and D.J.M. wrote the paper; and T.M., Ö.Ö., H.M.E-S., B.F., G.O., C.B., B.G., M.L., and
621 D.J.M. contributed to the revision and all authors approved the final submission.
622

623

References

1. Draganski B, Gaser C, Busch V, Schuierer G, Bogdahn U, May A. Neuroplasticity: changes in grey matter induced by training. Nature. 2004;427(6972):311-2.
2. Wenger E, Kuhn S, Verrel J, Martensson J, Bodammer NC, Lindenberger U, et al. Repeated Structural Imaging Reveals Nonlinear Progression of Experience-Dependent Volume Changes in Human Motor Cortex. Cereb Cortex. 2017;27(5):2911-25.
3. Keifer OP, Jr., Hurt RC, Gutman DA, Keilholz SD, Gourley SL, Ressler KJ. Voxel-based morphometry predicts shifts in dendritic spine density and morphology with auditory fear conditioning. Nat Commun. 2015;6:7582.
4. Kleim JA, Markham JA, Vij K, Freese JL, Ballard DH, Greenough WT. Motor learning induces astrocytic hypertrophy in the cerebellar cortex. Behav Brain Res. 2007;178(2):244-9.
5. Woo J, Min JO, Kang DS, Kim YS, Jung GH, Park HJ, et al. Control of motor coordination by astrocytic tonic GABA release through modulation of excitation/inhibition balance in cerebellum. Proc Natl Acad Sci U S A. 2018;115(19):5004-9.
6. McKenzie IA, Ohayon D, Li H, de Faria JP, Emery B, Tohyama K, et al. Motor skill learning requires active central myelination. Science. 2014;346(6207):318-22.
7. Keiner S, Niv F, Neumann S, Steinbach T, Schmeer C, Hornung K, et al. Effect of skilled reaching training and enriched environment on generation of oligodendrocytes in the adult sensorimotor cortex and corpus callosum. BMC Neurosci. 2017;18(1):31.
8. Kougioumtzidou E, Shimizu T, Hamilton NB, Tohyama K, Sprengel R, Monyer H, et al. Signalling through AMPA receptors on oligodendrocyte precursors promotes myelination by enhancing oligodendrocyte survival. Elife. 2017;6.
9. Zatorre RJ, Fields RD, Johansen-Berg H. Plasticity in gray and white: neuroimaging changes in brain structure during learning. Nat Neurosci. 2012;15(4):528-36.
10. Schmidt S, Gull S, Herrmann KH, Boehme M, Irintchev A, Urbach A, et al. Experience-dependent structural plasticity in the adult brain: How the learning brain grows. Neuroimage. 2021;225:117502.
11. Badea A, Ng KL, Anderson RJ, Zhang J, Miller MI, O'Brien RJ. Magnetic resonance imaging of mouse brain networks plasticity following motor learning. PLoS One. 2019;14(5):e0216596.
12. Sampaio-Baptista C, Khrapitchev AA, Foxley S, Schlagheck T, Scholz J, Jbabdi S, et al. Motor skill learning induces changes in white matter microstructure and myelination. J Neurosci. 2013;33(50):19499-503.
13. Sampaio-Baptista C, Valles A, Khrapitchev AA, Akkermans G, Winkler AM, Foxley S, et al. White matter structure and myelin-related gene expression alterations with experience in adult rats. Prog Neurobiol. 2020;187:101770.
14. Natu VS, Gomez J, Barnett M, Jeska B, Kirilina E, Jaeger C, et al. Apparent thinning of human visual cortex during childhood is associated with myelination. Proc Natl Acad Sci U S A. 2019;116(41):20750-9.
15. Weiskopf N, Suckling J, Williams G, Correia MM, Inkster B, Tait R, et al. Quantitative multi-parameter mapping of R1, PD(*), MT, and R2(*) at 3T: a multi-center validation. Front Neurosci. 2013;7:95.
16. Gibson EM, Purger D, Mount CW, Goldstein AK, Lin GL, Wood LS, et al. Neuronal activity promotes oligodendrogenesis and adaptive myelination in the mammalian brain. Science. 2014;344(6183):1252304.
17. Mensch S, Baraban M, Almeida R, Czopka T, Ausborn J, El Manira A, et al. Synaptic vesicle release regulates myelin sheath number of individual oligodendrocytes in vivo. Nat Neurosci. 2015;18(5):628-30.
18. Swire M, Ffrench-Constant C. Seeing Is Believing: Myelin Dynamics in the Adult CNS. Neuron. 2018;98(4):684-6.
19. Bacmeister CM, Barr HJ, McClain CR, Thornton MA, Nettles D, Welle CG, et al. Motor learning promotes remyelination via new and surviving oligodendrocytes. Nat Neurosci. 2020;23(7):819-31.

20. Wake H, Lee PR, Fields RD. Control of local protein synthesis and initial events in myelination by action potentials. Science. 2011;333(6049):1647-51.
21. Makinodan M, Rosen KM, Ito S, Corfas G. A critical period for social experience-dependent oligodendrocyte maturation and myelination. Science. 2012;337(6100):1357-60.
22. Geraghty AC, Gibson EM, Ghanem RA, Greene JJ, Ocampo A, Goldstein AK, et al. Loss of Adaptive Myelination Contributes to Methotrexate Chemotherapy-Related Cognitive Impairment. Neuron. 2019;103(2):250-65 e8.
23. Pan S, Mayoral SR, Choi HS, Chan JR, Kheirbek MA. Preservation of a remote fear memory requires new myelin formation. Nat Neurosci. 2020;23(4):487-99.
24. Steadman PE, Xia F, Ahmed M, Mocle AJ, Penning ARA, Geraghty AC, et al. Disruption of Oligodendrogenesis Impairs Memory Consolidation in Adult Mice. Neuron. 2020;105(1):150-64.e6.
25. Kleim JA, Barbay S, Nudo RJ. Functional reorganization of the rat motor cortex following motor skill learning. J Neurophysiol. 1998;80(6):3321-5.
26. Kleim JA, Hogg TM, VandenBerg PM, Cooper NR, Bruneau R, Remple M. Cortical synaptogenesis and motor map reorganization occur during late, but not early, phase of motor skill learning. J Neurosci. 2004;24(3):628-33.
27. Tennant KA, Adkins DL, Donlan NA, Asay AL, Thomas N, Kleim JA, et al. The organization of the forelimb representation of the C57BL/6 mouse motor cortex as defined by intracortical microstimulation and cytoarchitecture. Cereb Cortex. 2011;21(4):865-76.
28. Xu T, Yu X, Perlik AJ, Tobin WF, Zweig JA, Tennant K, et al. Rapid formation and selective stabilization of synapses for enduring motor memories. Nature. 2009;462(7275):915-9.
29. Hill RA, Patel KD, Goncalves CM, Grutzendler J, Nishiyama A. Modulation of oligodendrocyte generation during a critical temporal window after NG2 cell division. Nat Neurosci. 2014;17(11):1518-27.
30. Whishaw IQ, O'Connor WT, Dunnett SB. The contributions of motor cortex, nigrostriatal dopamine and caudate-putamen to skilled forelimb use in the rat. Brain. 1986;109 (Pt 5):805-43.
31. Kim JS, Lee HJ, Lee S, Lee HS, Jeong YJ, Son Y, et al. Conductive Hearing Loss Aggravates Memory Decline in Alzheimer Model Mice. Front Neurosci. 2020;14:843.
32. Sawiak SJ, Wood NI, Williams GB, Morton AJ, Carpenter TA. Voxel-based morphometry in the R6/2 transgenic mouse reveals differences between genotypes not seen with manual 2D morphometry. Neurobiol Dis. 2009;33(1):20-7.
33. Bagdatlioglu E, Porcari P, Greally E, Blamire AM, Straub VW. Cognitive impairment appears progressive in the mdx mouse. Neuromuscul Disord. 2020;30(5):368-88.
34. Ashburner J, Friston KJ. Voxel-based morphometry--the methods. Neuroimage. 2000;11(6 Pt 1):805-21.
35. Jung WB, Shim HJ, Kim SG. Mouse BOLD fMRI at ultrahigh field detects somatosensory networks including thalamic nuclei. Neuroimage. 2019;195:203-14.
36. Bechler ME, Swire M, Ffrench-Constant C. Intrinsic and adaptive myelination-A sequential mechanism for smart wiring in the brain. Dev Neurobiol. 2018;78(2):68-79.
37. Xiao L, Ohayon D, McKenzie IA, Sinclair-Wilson A, Wright JL, Fudge AD, et al. Rapid production of new oligodendrocytes is required in the earliest stages of motor-skill learning. Nat Neurosci. 2016;19(9):1210-7.
38. Buetefisch CM, Revill KP, Shuster L, Hines B, Parsons M. Motor demand-dependent activation of ipsilateral motor cortex. J Neurophysiol. 2014;112(4):999-1009.
39. Wischnewski M, Kowalski GM, Rink F, Belagaje SR, Haut MW, Hobbs G, et al. Demand on skillfulness modulates interhemispheric inhibition of motor cortices. J Neurophysiol. 2016;115(6):2803-13.
40. Wenger E, Brozzoli C, Lindenberger U, Lovden M. Expansion and Renormalization of Human Brain Structure During Skill Acquisition. Trends Cogn Sci. 2017;21(12):930-9.
41. Makino H, Hwang EJ, Hedrick NG, Komiyama T. Circuit Mechanisms of Sensorimotor Learning. Neuron. 2016;92(4):705-21.
42. Lindenberger U, Lövdén M. Brain Plasticity in Human Lifespan Development: The Exploration–Selection–Refinement Model. Annual Review of Developmental Psychology. 2019;1(1):197-222.

43. Milner B, Squire LR, Kandel ER. Cognitive neuroscience and the study of memory. Neuron. 1998;20(3):445-68.
44. Yang SM, Michel K, Jokhi V, Nedivi E, Arlotta P. Neuron class-specific responses govern adaptive myelin remodeling in the neocortex. Science. 2020;370(6523).
45. Kilgard MP. Harnessing plasticity to understand learning and treat disease. Trends Neurosci. 2012;35(12):715-22.
46. Bonetto G, Belin D, Karadottir RT. Myelin: A gatekeeper of activity-dependent circuit plasticity? Science. 2021;374(6569):eaba6905.
47. Chung S, Wang X, Lui YW. Influence of T1-Weighted Signal Intensity on FSL Voxel-Based Morphometry and FreeSurfer Cortical Thickness. AJNR Am J Neuroradiol. 2017;38(4):726-8.
48. Molina-Luna K, Pekanovic A, Rohrich S, Hertler B, Schubring-Giese M, Rioult-Pedotti MS, et al. Dopamine in motor cortex is necessary for skill learning and synaptic plasticity. PLoS One. 2009;4(9):e7082.
49. Saab BJ, Maclean AJ, Kanisek M, Zurek AA, Martin LJ, Roder JC, et al. Short-term memory impairment after isoflurane in mice is prevented by the alpha5 gamma-aminobutyric acid type A receptor inverse agonist L-655,708. Anesthesiology. 2010;113(5):1061-71.
50. Delora A, Gonzales A, Medina CS, Mitchell A, Mohed AF, Jacobs RE, et al. A simple rapid process for semi-automated brain extraction from magnetic resonance images of the whole mouse head. J Neurosci Methods. 2016;257:185-93.
51. Tustison NJ, Avants BB, Cook PA, Zheng Y, Egan A, Yushkevich PA, et al. N4ITK: improved N3 bias correction. IEEE Trans Med Imaging. 2010;29(6):1310-20.
52. Hikishima K, Komaki Y, Seki F, Ohnishi Y, Okano HJ, Okano H. In vivo microscopic voxel-based morphometry with a brain template to characterize strain-specific structures in the mouse brain. Sci Rep. 2017;7(1):85.
53. Sawiak SJ, Wood NI, Williams GB, Morton AJ, Carpenter TA. Voxel-based morphometry with templates and validation in a mouse model of Huntington's disease. Magn Reson Imaging. 2013;31(9):1522-31.
54. Bates D, Mächler M, Bolker B, Walker S. Fitting Linear Mixed-Effects Models Using lme4. 2015. 2015;67(1):48.
55. Barriere DA, Ella A, Szeremeta F, Adriaensen H, Meme W, Chaillou E, et al. Brain orchestration of pregnancy and maternal behavior in mice: A longitudinal morphometric study. Neuroimage. 2021;230:117776.
56. Schindelin J, Arganda-Carreras I, Frise E, Kaynig V, Longair M, Pietzsch T, et al. Fiji: an open-source platform for biological-image analysis. Nat Methods. 2012;9(7):676-82.
57. Liao PS, Chew TS, Chung PC. A fast algorithm for multilevel thresholding. J Inf Sci Eng. 2001;17(5):713-27.

Supplementary Information for:

Learning-related contraction of grey matter in rodent sensorimotor cortex is associated with adaptive myelination

Tomas Mediavilla, Özgün Özalay, Héctor M. Estévez-Silva, Bárbara Frías, Greger Orädd, Fahad R. Sultan, Claudio Brozzoli, Benjamín Garzón, Martin Lövdén and Daniel J. Marcellino*

[a] Department of Integrative Medical Biology, Umeå University, 90 187 - Umeå, Sweden

[b] Aging Research Center, Department of Neurobiology, Care Sciences and Society, Karolinska Institute, 17 165 - Solna, Sweden

[c] Department of Psychology, University of Gothenburg, 405 30 - Gothenburg, Sweden

***Corresponding author**

Email: daniel.marcellino@umu.se

Supplementary Information includes:

Figures S1 to S8
Tables S1
Legends for Movies S1

Other supplementary materials for this manuscript include the following:

Movies S1

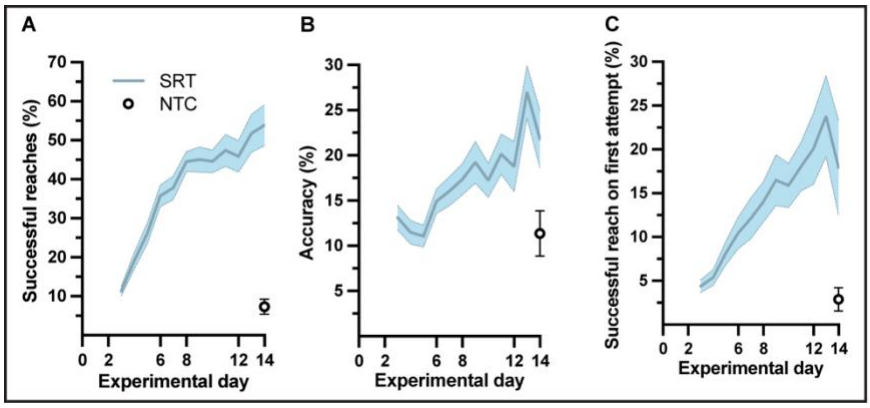

Fig. S1. Mean performance scores of animals used for a cross-sectional myelin immunoreactivity during learning of a skilled, single-pellet forelimb reach task. Performace calculated as percentage (54 ± 5) of successful reaches (***A***) and percent (22 ± 3) accuracy (***B***) or percentage of successful reaches on the first attempted reach (***C***), during the 12-day training paradigm.

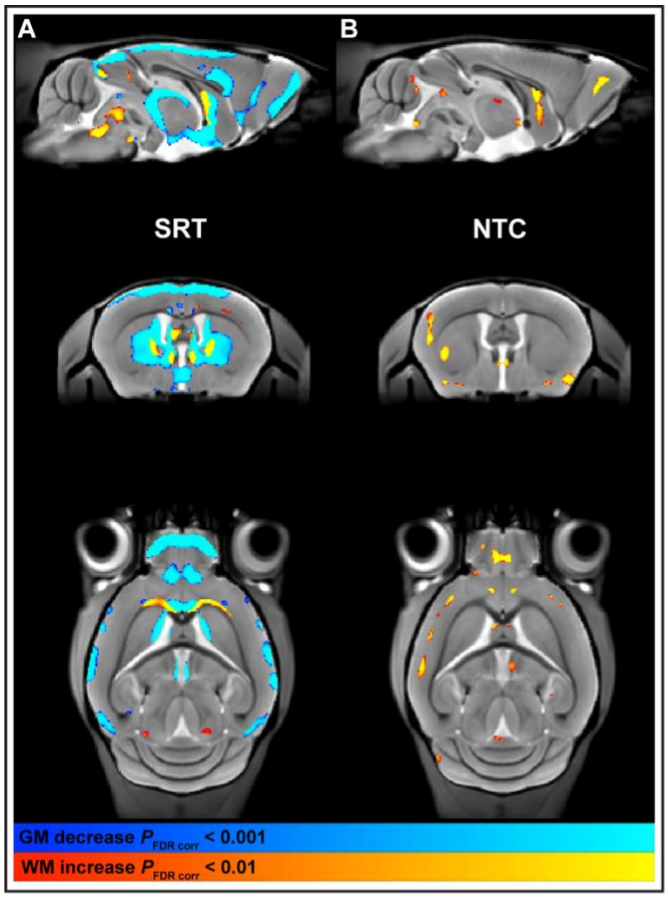

Fig. S2. Forelimb reach-and-grasp training dynamically modulates macrostructural brain plasticity. Training mice in the single-pellet forelimb reach task produces non-linear decreases in grey matter volume (GMV) ($P_{FDR\ corr}$ < 0.001) and non-linear increases in white matter volume (WMV) ($P_{FDR\ corr}$ < 0.01) (***A***), whereas a linear increase in GMV was observed in non-trained control animals with time (***B***), whole-brain statistical maps ($P_{FDR\ corr}$ < 0.01) are represented on a study-specific *in vivo* template (AP -0.1 mm, DV -3.0 mm from Bregma; 0.08 mm isotropic, radiological display).

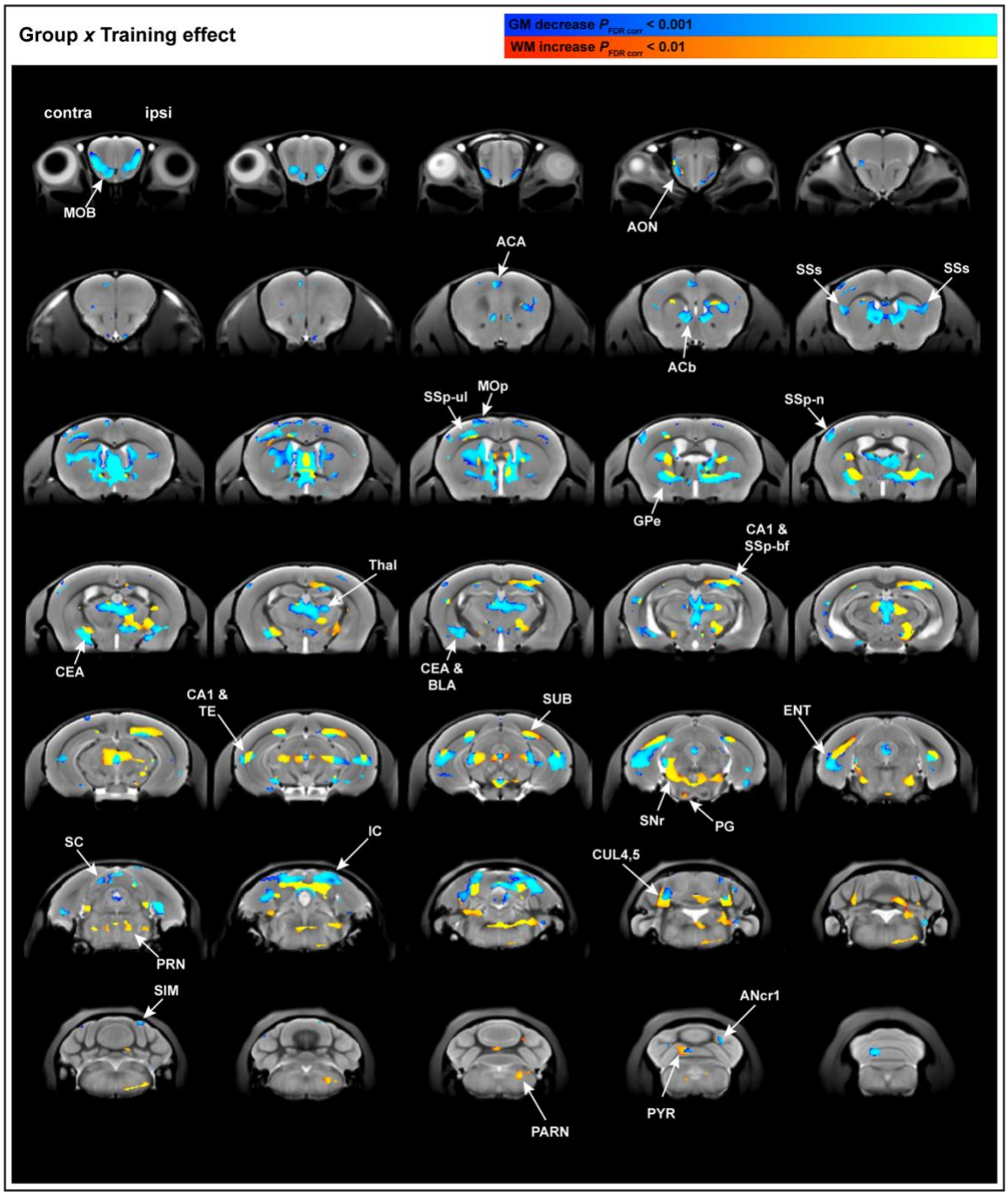

Fig. S3. Whole brain structural analysis of non-linear decreases in grey matter volume juxtaposed to non-linear increases in white matter volume with learning. Changes in GMV and WMV modelled using the asymptotic model and overlayed on the *in vivo* MRI template created from this study. Whole-brain decreases in GMV (cold blue scale) and the increases in WMV (warm red scale), in coronal sections ranging from A/P Bregma -4.3 to -7.5 mm.

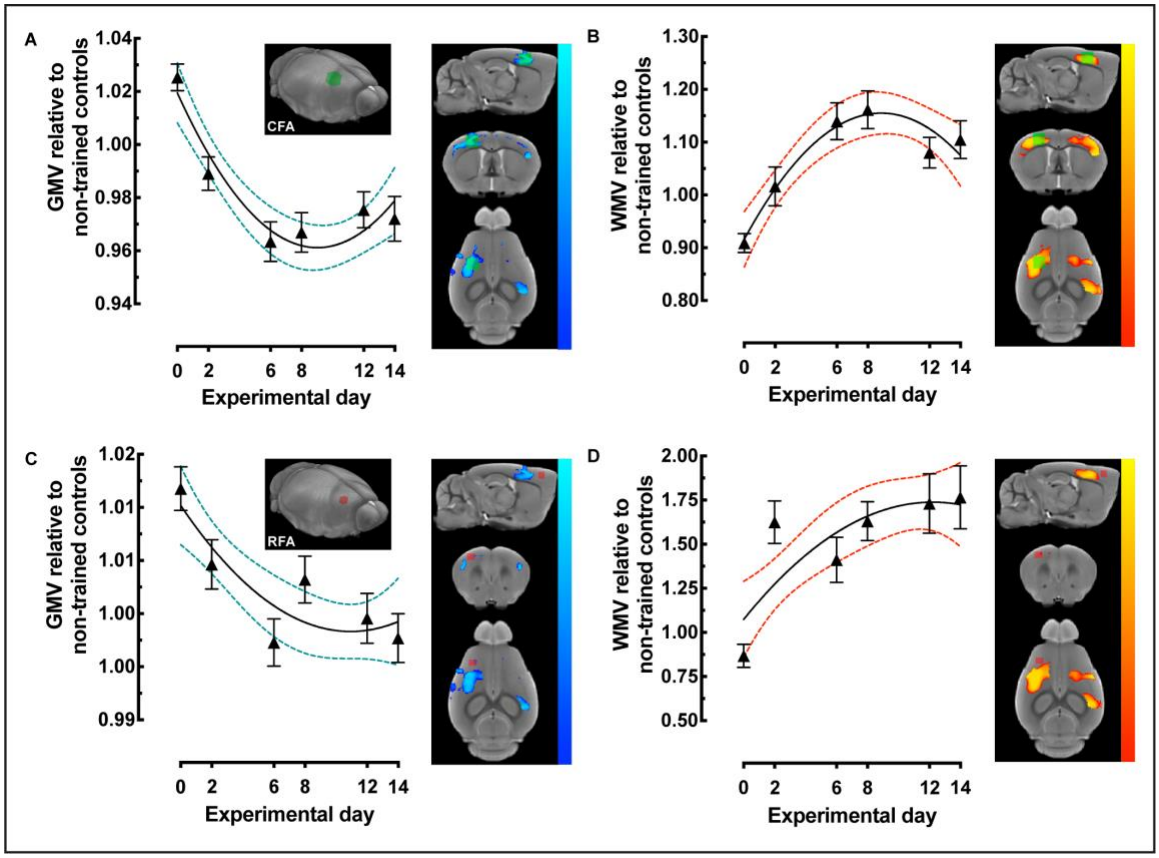

Fig. S4. CFA- and RFA-restricted VBM analysis identified non-linear decreases in GMV together with non-linear increases in WMV during motor learning. ***A***, GMV, relative to non-trained controls, in CFA contralateral to the trained forelimb (VOI represented in green). ***B***, WMV extracted and plotted from CFA VOI in ***A***. ***C***, GMV, relative to non-trained controls, in RFA contralateral to the trained forelimb (VOI represented in red). ***B***, WMV extracted and plotted from the same RFA VOI in ***C***.

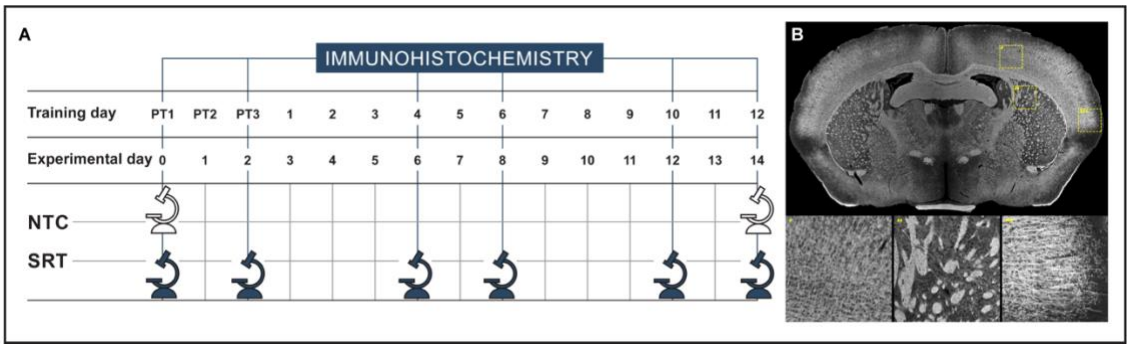

Fig. S5. Experimental design for the cross-sectional immunohistochemistry analysis of myelin immunoreactivity (***A***) and representative image of myelin basic protein immunohistochemistry (***B***) highlighting the specificity of the immunodetection of myelin in cortex and striatum.

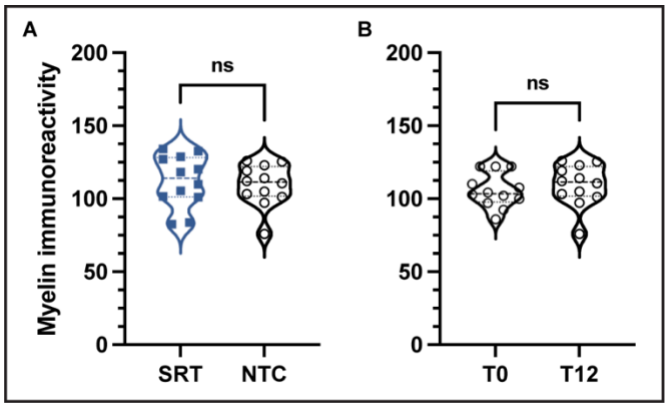

Fig. S6. There are no differences in myelin immunoreactivity between trained animals and non-trained control animals (***A***) at the last training day (training day 12). In addition, no differences in myelin immunoreactivity were observed between non-trained control animals at experimental day 0 and at training day 12 (***B***).

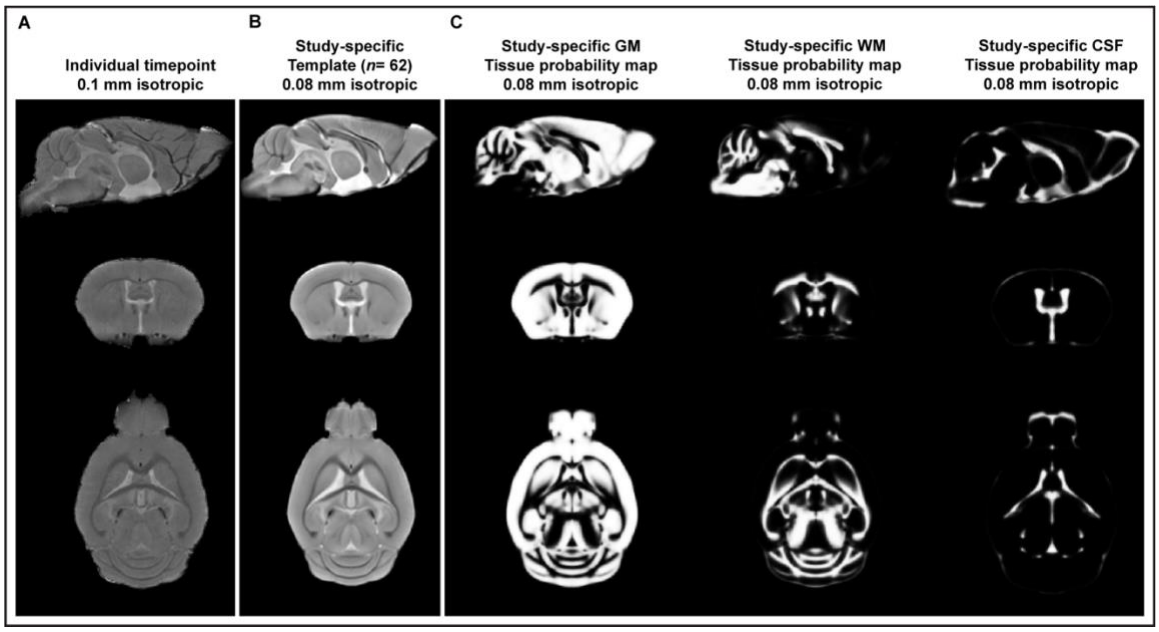

Fig. S7. Sagittal, coronal, and horizontal sections of an *in vivo* microscopic T1-weighted image from one individual scan during the longitudinal study (***A***) and the study-specific template created for mouse brain (***B***). Study- and MR sequence-specific brain tissue probability maps (***C***). Sagittal, coronal, and horizontal sections of tissue probability maps (TPMs) of grey matter (GM), white matter (WM), cerebrospinal fluid (CSF).

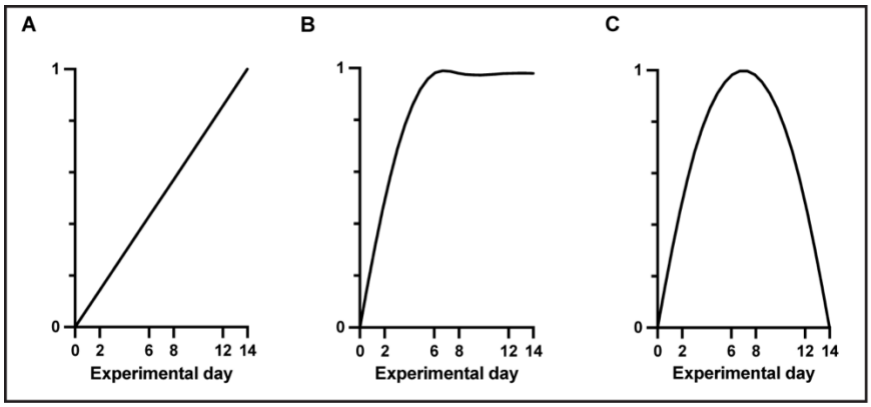

Fig. S8. Three different regression models representing three different time-courses were used to test for different patterns of change in GM and WM; ***(A)*** Linear, (***B***) Increase followed by a stabilization (inverse-quadratic-asymptotic), and (***C***) Increase followed by a renormalization (inverse-quadratic).

Table S1. Effect of training on grey and white matter in trained mice and the effect of time in non-trained control mice. Whole-brain within-group analysis presenting the significant number of voxels ($P_{FDR\ corr.}$ < 0.01 and < 0.001) together with the change in volume (mm^3).

grey matter (GM) changes				
	Trained mice (*n* = 39)		Non-trained controls (*n* = 16)	
	increase	decrease	increase	decrease
$P_{FDR\ corr}$ < 0.01				
Linear	-	-	29327 (15.02)	-
Asymptotic	2832 (1.45)	139233 (71.29)	-	-
Quadratic	-	39493 (20.22)	-	-
$P_{FDR\ corr}$ < 0.001				
Linear	-	-	14316 (7.33)	-
Asymptotic	1643 (0.84)	97106 (46.72)	-	-
Quadratic	-	15477 (7.91)	-	-
white matter (WM) changes				
	Trained mice (*n* = 39)		Non-trained controls (*n* = 16)	
	increase	decrease	increase	decrease
$P_{FDR\ corr}$ < 0.01				
Linear	-	-	-	-
Asymptotic	26453 (13.54)	2510 (1.29)	-	-
Quadratic	91 (0.05)	-	-	-
$P_{FDR\ corr}$ < 0.001				
Linear	-	-	-	-
Asymptotic	16590 (6.96)	1196 (0.61)	-	-
Quadratic	-	-	-	-

Movie S1. A forelimb-specific motor learning paradigm (single pellet skilled reaching task) providing examples of successful skilled reaches as well as unsuccessful attempts to reach and grasp the pellet.